Journal of Molecular Graphics and Modelling 29 (2010) 354–362

Contents lists available at ScienceDirect

Journal of Molecular Graphics and Modelling

journal homepage: www.elsevier.com/locate/JMGM

Theoretical studies on the interactions of XIAP-BIR3 domain with bicyclic and tricyclic core monovalent Smac mimetics

Baoping Ling[a], Lihua Dong[b,c], Rui Zhang[b], Zhiguo Wang[b], Yongjun Liu[a,b,*], Chengbu Liu[a]

[a] Key Lab of Colloid and Interface Chemistry, Ministry of Education, School of Chemistry and Chemical Engineering, Shandong University, Jinan, Shandong 250100, China
[b] Northwest Institute of Plateau Biology, Chinese Academy of Sciences, Xining, Qinghai 810001, China
[c] School of Chemistry and Chemical Engineering, Taishan Medical University, Taian, Shandong 270000, China

ARTICLE INFO

Article history:
Received 7 July 2010
Received in revised form
14 September 2010
Accepted 23 September 2010
Available online 25 October 2010

Keywords:
Smac mimetics
Caspase-9
XIAP-BIR3
Molecular docking
Molecular dynamics simulations
Binding free energy

ABSTRACT

X-linked IAP can bind caspase-9 and inhibit its activity. Mitochondrial protein Smac/DIABLO can also interact with XIAP and relieve the inhibition on caspase-9 to induce apoptosis. A series of artificial Smac mimetics have been used to mimic the Smac N-terminal tetrapeptide AVPI to bind to XIAP-BIR3, but these structural diverse mimetics exhibited distinct binding affinities. To get an insight into the binding nature and optimize the structures, molecular docking and dynamics simulations were used to study the binding of XIAP-BIR3 with three groups of Smac mimetics. The docking results reveal that these Smac mimetics anchored on the surface groove of XIAP-BIR3 and superimposed well with AVPI. The modifications on the seven-membered ring of bicyclic core segment do not strengthen the binding affinity, while a benzyl introduced to the five-membered ring is favorable to the binding. Molecular dynamics simulations on three typical systems show that these complexes are very stable. Hydrogen bonds between the bicyclic core segment and Thr308 play critical roles in maintaining the stability of complex. The binding free energies calculated by MM_PBSA method are consistent with the experimental results.

1. Introduction

Mitochondria-mediated apoptosis plays an essential role in normal proliferation and development of multicellular organisms, and inappropriate apoptotic regulation could lead to a number of diseases [1,2]. There are "intrinsic" and "extrinsic" two major apoptotic pathways which are executed by the initiator and effector caspases [3]. Caspases are a class of cysteine-aspartyl proteases and typically lie dominantly in healthy cell in response to cell death stimulus [4].

IAPs are the key apoptosis regulators which interact with caspase and suppress cell death [5]. XIAP contains three baculoviral IAP repeat (BIR) domains, each BIR domain exhibits distinct function, and the third BIR domain (XIAP-BIR3) inhibits apoptosis through selectively targeting caspase-9 [6,7]. Whereas, a mitochondrial protein Smac/DIABLO is an endogenous antagonist of IAPs, and can also bind to the surface groove in XIAP-BIR3 domain to relieve their inhibitory effect on caspase-9 and induce apoptosis [8,9].

Smac interacts with XIAP-BIR3 through the N-terminal tetrapeptide AVPI sequence [10–12]. On the basis of crystal structures, many groups have designed and synthesized a series of peptidic and nonpeptidic Smac mimetics [13–18]. Recently, two types of Smac mimetics, monovalent and divalent, have been reported and both of them are great potential anticancer drugs [19–21]. Since monovalent Smac mimetics are of lower molecular weight and good bioavailability, intense efforts have focused on designing and synthesizing monovalent mimetics [22], of which Wang's groups reported a number of conformationally constrained bicyclic Smac mimetics [22–25]. To improve the cell activity of these mimetics, they modified them by using a structure-based approach to generate a series of new anticancer drugs [26–28]. They found these structurally diverse mimetics exhibited distinct cell activity. For example, when a phenyl was fused to the seven-membered ring to obtain tricyclic core Smac mimetics, the compounds with R- and S-tetrahydronaphthyl group correspond to different inhibition constant (Ki) (18 *vs* 1200 nM) and IC_{50} (68 *vs* 401 nM) [26]. A minute change of structure may cause a great loss of binding affinity and cell activity.

Although Wang's groups have predicted the binding sites of some Smac mimetics by molecular modeling [26,28], and Yang et al. have calculated the binding free energy of some mimetics [29], the specific binding modes and different structural effect on the binding were not addressed. We previously reported the mechanism of bicyclic core Smac mimetics interacting with XIAP-BIR3

Abbreviations: Smac, second mitochondria-derived activator of caspases, also named DIABLO, a direct IAP binding protein with low *PI*; AVPI, Ala1-Val2-Pro3-Ile4; IAP, inhibitors of apoptosis protein; XIAP, X-linked inhibitor of apoptosis protein; BIR3, the third baculoviral IAP repeats domain.

* Corresponding author at: Theoretical Chemistry, School of Chemistry and Chemical Engineering, No. 27 Shan Da Nan Lu, Jinan, Shandong 250100, China.
Tel.: +86 531 88365576; fax: +86 531 885 644 64.
E-mail address: yongjunliu_1@sdu.edu.cn (Y. Liu).

1093-3263/$ – see front matter © 2010 Elsevier Inc. All rights reserved.
doi:10.1016/j.jmgm.2010.09.011

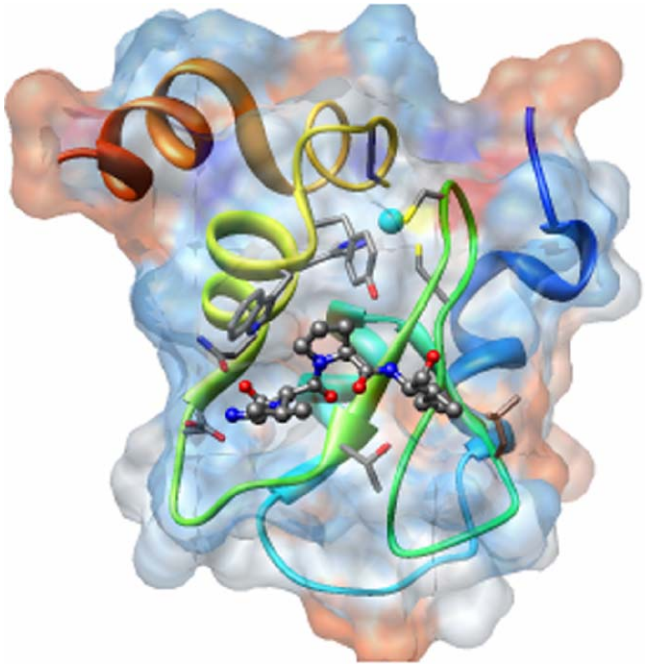

Fig. 1. The Smac N-terminal tetrapeptide AVPI on the hydrophobic surface of XIAP-BIR3 domain (PDB code: 1G73, Chain C). AVPI is shown in ball and stick. The zinc ion is colored cyan and shown in ball. The hydrophobic surface shows the amino acid hydrophobicity with colors ranging from dodger blue for the most hydrophilic to white at 0.0 to orange red for the most hydrophobic. (For interpretation of the references to color in this figure legend, the reader is referred to the web version of the article.)

Table 1
Chemical structures of selected Smac mimetics in this study.

Mimetics	Chemical structures	Mimetics	Chemical structures
SMa1	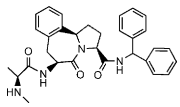	SMa2	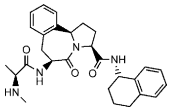
SMa3	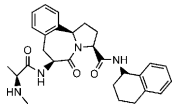	SMa4	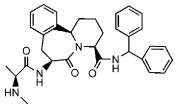
SMb1	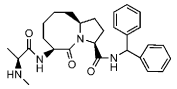	SMb2	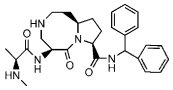
SMb3	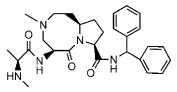	SMb4	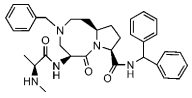
SMb5	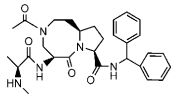	SMb6	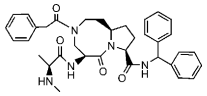
SMc1	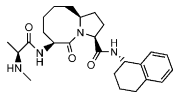	SMc2	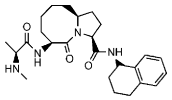
SMc3	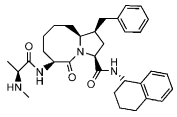	SMc4	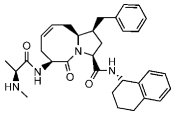

Note: The SMa mimetics are from Ref. [26], SMb mimetics are from Ref. [27] and SMc mimetics are from Ref. [28].

domain [30], which indicated that the bicyclic core segments of mimetics play important roles for ligand binding, and only one of two terminal phenyls locates in the hydrophobic pocket. However, how the modifications on the bicyclic core segments and terminal groups affect the interactions between Smac mimetics and XIAP-BIR3 has not been discussed theoretically in detail. Based on the modifications on the bicyclic core segment and terminal group of mimetics designed by Wang's group [26–28], we used docking and molecular dynamics simulations to investigate the interactions of these mimetics with XIAP-BIR3, and gained an insight into the effect of structural variations of bicyclic core segments on their binding affinity and binding modes, which may be helpful for designing and synthesizing novel anticancer drugs.

2. Computational details

The coordinate of XIAP-BIR3 was downloaded from Brookhaven Protein Data Bank (www.rcsb.org). The PDB entry is 1G73 with resolution of 2.0 Å, and the crystal structure is dimeric polymer, so we select chain C to sever as receptor and the three-dimensional structure is shown in Fig. 1. The chemical structures of Smac mimetics are shown in Table 1, which are taken from the experiments of Wang's groups [26–28]. Geometries of Smac mimetics were fully optimized using Gaussian 03 program [31] at the level of B3LYP/6-31G. Before docking, all the substances except receptor were removed, and AutoDockTools [32] were applied to add the polar hydrogen atoms and assign Kollman united atom partial charges to the receptor.

2.1. Molecular docking

AutoDock4.0 program [32] was used for docking calculations combined with Lamarckian genetic algorithm (LGA) to search for the preferable conformation. The center of the grid box was set to residue Leu307, and the size of box was $60 \times 60 \times 60$ grid point with grid spacing of 0.375 Å. During the docking experiment, the receptor was kept rigid and ligand was set flexible. The maximum number of energy evaluations was set to 2.5×10^7, and the rest of docking parameters were used the default values. 50 independent docking runs were performed to find the preferable conformation. The docking results were clustered according to the root mean square deviation (RMSD) of 2.0 Å. The structures with the relative lower binding free energy and the most cluster members were chosen, which were subjected to the following molecular dynamics (MD) simulations [33].

2.2. Energy minimization and molecular dynamics

All the MD simulations of complexes were carried out in amber99 force field in NTP ensemble [34]. The complexes were solvated in a 56.2 Å × 56.2 Å × 56.2 Å box with periodic boundary condition by adding TIP3P water molecules, and two sodium ions were added to neutralize each system. Long-range electrostatic interaction was calculated using the particle mesh Ewald (PME) method with a cut-off of 9 Å. All bonds involving hydrogen bonds were constrained with the SHAKE algorithm. The systems were firstly energy minimized for 1500 steps with the conjugate gradient and steepest descent algorithm, respectively. Then, the position-restrained MD simulations were carried out for 250 ps, afterwards, 5 ns MD simulations were run at a time step of 0.2 ps. The dynamics trajectories were saved every 2 ps for analysis [35,36]. The zinc ion was treated by using cationic dummy atom method which was successfully employed to calculate the proteins containing zinc ions [37,38].

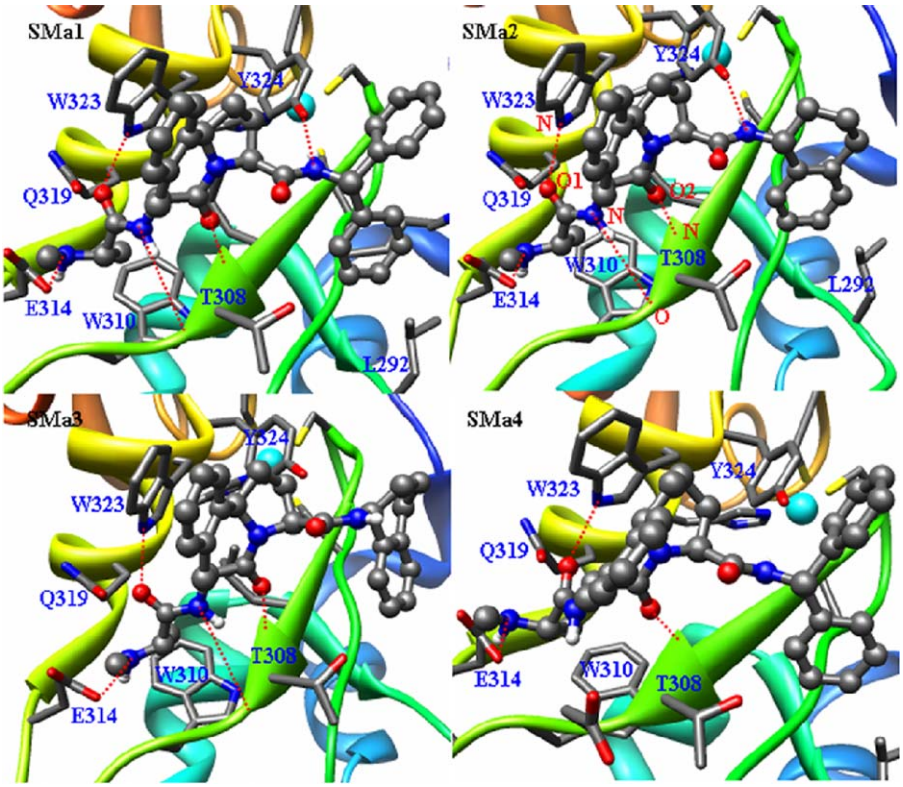

Fig. 2. The docking conformations of tricyclic core Smac mimetics bound to XIAP-BIR3. The red dashed lines represent hydrogen bonds. (For interpretation of the references to color in this figure legend, the reader is referred to the web version of the article.)

2.3. Binding free energy calculation

MM_PBSA method [39] was used to calculate the binding free energy of complex, and 50 snapshots were extracted from the single molecular dynamics trajectory. For entropic contribution, it is computationally expensive, so we extracted 10 snapshots to estimate the entropy. The binding free energy calculated by MM_PBSA method is described as the follows [40]:

$$\Delta G_{\text{bind}} = G_{\text{com}} - (G_{\text{pro}} + G_{\text{lig}}) \quad (1)$$

$$G = E_{\text{MM}} + G_{\text{sol}} - \text{TS} \quad (2)$$

$$E_{\text{MM}} = E_{\text{INT}} + E_{\text{VDW}} + E_{\text{ELE}} \quad (3)$$

$$G_{\text{sol}} = G_{\text{PB}} + G_{\text{np}} \quad (4)$$

$$G_{\text{np}} = a\text{SASA} + b \quad (5)$$

where ΔG_{bind} accounts for the binding free energy, G_{com}, G_{pro} and G_{lig} represent the free energy of complex, protein and ligand, respectively. Each term is composed of the total energy obtained by molecular mechanic in gas phase (E_{MM}), solvent free energy (G_{sol}) and entropy term (–TS). E_{MM} includes internal energy (E_{INT}), van der Waals (E_{VDW}) as well as electrostatic energy (E_{ELE}). The solvent free energy G_{sol} is decomposed into polar contribution (G_{PB}) and non-polar contribution (G_{np}) to solvation. G_{PB} is obtained by solving Poisson–Boltzmann equation, and the dielectric constant is set to 80.0 for the surrounding solvent while 1.0 for the solute. G_{np} is determined with solvent-accessible-surface-area (SASA) dependent terms and calculated by LCPO method with $a = 0.00542$ kcal/mol Å^{-2} and $b = 0.92$ kcal/mol, respectively [41]. The entropic contribution is computed through a normal mode analysis.

3. Results and discussions

3.1. Docking results

According to the structures of Smac mimetics listed in Table 1, we divided them into three groups, namely SMa, SMb and SMc. In SMa, a phenyl is fused to the seven-membered ring to obtain tricyclic core Smac mimetics [26]. In SMb, the original seven-membered ring of bicyclic core is replaced by an eight-membered ring with different substitutes [27]. In SMc, a benzyl group is introduced on the five-membered ring, and the terminal diphenylmethyl group is substituted by R- or S-tetrahydronaphthyl [28].

3.1.1. SMa

The docking results in Fig. 2 show that SMa mimetics bind to XIAP-BIR3 with the “extended” conformations, i.e., one phenyl of diphenylmethyl locates in the hydrophobic pocket and the other phenyl extends to the surrounding solvent, which is similar to the experimental results of four-substituted azabicyclo[5,3,0] alkane mimetics and compound 21 carried out by Mastrangelo and Sun [22,42]. All the 3D figures in this study were created by Chimera program [43].

From the docking conformations, we can see that the phenyl rings of SMa parallel to the indole ring of Trp323, which does not affect the original hydrogen bonds. The calculated K_i values are approximate to the experimental data and the tendencies are the same (see Table 2). Compared to SM-131 without a phenyl on seven-membered ring [25], the binding energy of SMa1 (−10.21 kcal/mol) is comparable to that of SM-131 (−10.24 kcal/mol), i.e., the phenyl provides little contribution to the binding energy. The experimental studies showed that the inhibition constant K_i of SMa1 was a little lower than that of SM-131 (30 *vs* 61 nM) [26], which indirectly validated our calculation is reliable.

Table 2
Diverse energies (kcal/mol) of Smac mimetics bound to XIAP-BIR3 by docking.

Smac	Vdw + Hbond + desolv	Electrostatic energy	Binding energy	K_i (nM)	$K_{i,exp}$ (nM)	$IC_{50,exp}$ (nM)
SMa1	−10.11	−1.87	−10.21	33	30[a]	468[a]
SMa2	−9.96	−1.90	−10.52	19	18[a]	68[a]
SMa3	−10.24	−0.15	−8.90	302	1200[a]	401[a]
SMa4	−9.48	−1.92	−9.61	91	690[a]	1369[a]
SMb1	−9.65	−1.76	−9.32	147	26[b]	259[b]
SMb2	−9.37	−1.66	−8.94	281	20[b]	890[b]
SMb3	−9.38	−1.66	−8.96	273	341[b]	1300[b]
SMb4a	−10.05	−1.76	−9.13	204	91.8[b]	1000[b]
SMb4b	−10.29	−1.51	−9.12	206		
SMb5a	−9.48	−1.66	−9.05	232	5.4[b]	69[b]
SMb5b	−10.38	−1.56	−9.85	61		
SMb6a	−9.08	−1.69	−8.08	1200	8.4[b]	31[b]
SMb6b	−10.60	−1.46	−9.37	135		
SMc1	−9.20	−1.94	−10.00	47	14[c]	73[c]
SMc2	−9.66	−1.75	−9.92	54	209[c]	1800[c]
SMc3	−11.96	−1.79	−11.66	2.8	3.9[c]	8.9[c]
SMc4	−11.84	−1.82	−11.57	3.3	31[c]	26[c]

[a] The data are from Ref. [26].
[b] The data are from Ref. [27].
[c] The data are from Ref. [28].

A tetrahydronaphthyl group was introduced such as in SMa2 and SMa3 (SMa2 and SMa3 are R- and S- isomer, respectively) to study the influence of terminal substituent on the hydrophobic interaction. The calculating results reveal that both of the tetrahydronaphthyl groups of the two isomers locate in the hydrophobic pocket, but the binding energy of SMa2 (−10.52 kcal/mol) is more negative than that of SMa3 (−8.90 kcal/mol), which is mainly caused by the electrostatic interaction (−1.90 *vs* −0.15 kcal/mol). In addition, for SMa2, the nitrogen of terminus forms an additional hydrogen bond with the oxygen of Tyr324, and the R-tetrahydronaphthyl is close to the hydrophobic residues Leu292 and Val298 to form stronger hydrophobic interaction. Accordingly we can deduce that the R-tetrahydronaphthyl group is more beneficial to the binding.

However, when a six-membered ring replaces the five-membered ring such as in SMa4, the original hydrogen bond between the nitrogen atom of imide and oxygen atom of Thr308 vanished, and the seven-membered ring keeps away from the indole ring of Trp323, resulting in the loss of the binding energy (−10.21 *vs* −9.61 kcal/mol).

3.1.2. SMb

Peng et al. synthesized some bicyclic core Smac mimetics, in which the seven-membered ring was replaced by eight-membered ring as shown in Table 1 [27]. We performed docking on these mimetics and the docking results are given in Figs. 3 and 4. By comparing Fig. 3 and Fig. 2, one can see that the eight-membered ring show little influence on the hydrogen bonds to Thr308, but the amino terminus forms an additional hydrogen bond. From an energetic standpoint, the binding energies are more positive than those of SMa mimetics (except SMa3 with S-tetrahydronaphthyl) in Table 2. We can deduce that the eight-membered ring is unfavorable to the binding. Moreover, the binding energy changes from −9.32 to −8.94 kcal/mol after the carbon atom in the eight-membered ring was replaced by nitrogen atom.

A benzyl, acetyl or phenylacetyl group was also introduced to the nitrogen atom in eight-membered ring such as in SMb4, SMb5 and SMb6 to value the steric exclusion. In Fig. 4, each mimetic corresponds to two docking conformations that differ in the orientations of the substituents, in which the substituent closes to the indole of Trp323 or Thr308, respectively. For SMb4, the two different conformations (SMb4a and SMb4b) correspond to the equal binding energies (Table 2). But SMb5 and SMb6 show different situations. The binding energies of SMb5a and SMb6a are less negative than those of SMb5b and SMb6b (−9.05 *vs* −9.85 and −8.08 *vs* −9.37 kcal/mol), respectively.

3.1.3. SMc

The docking results are given in Fig. 5. It can be seen that both the tetrahydroaphthyl groups of SMc1 and SMc2 locate in the hydrophobic pocket, and their orientations are consistent with those of SMa2 and SMa3 in Fig. 2, respectively. The number of hydrogen bonds of SMc1 is less than that of SMc2, but the electrostatic interaction of SMc1 is stronger, overall the binding affinity of SMc1 is slightly stronger than that of SMc2, i.e., R-

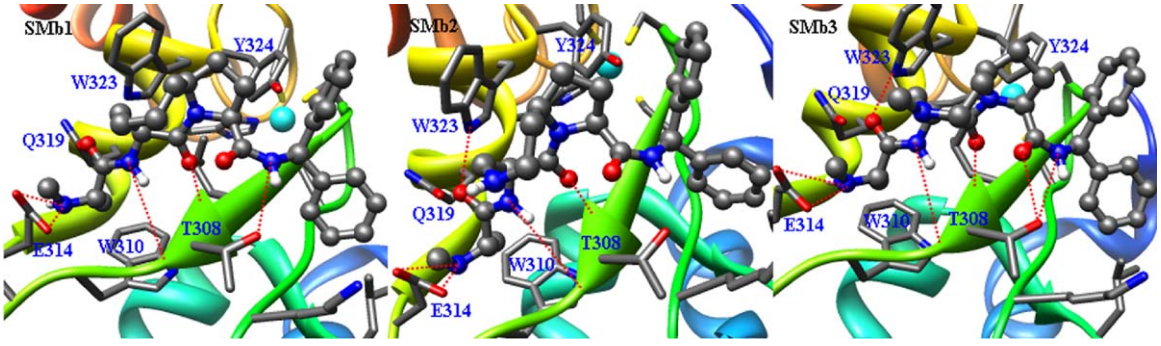

Fig. 3. The docking conformations of bicyclic core Smac mimetics with eight-membered ring SMb(1–3) bound to XIAP-BIR3. The red dashed lines represent hydrogen bonds. (For interpretation of the references to color in this figure legend, the reader is referred to the web version of the article.)

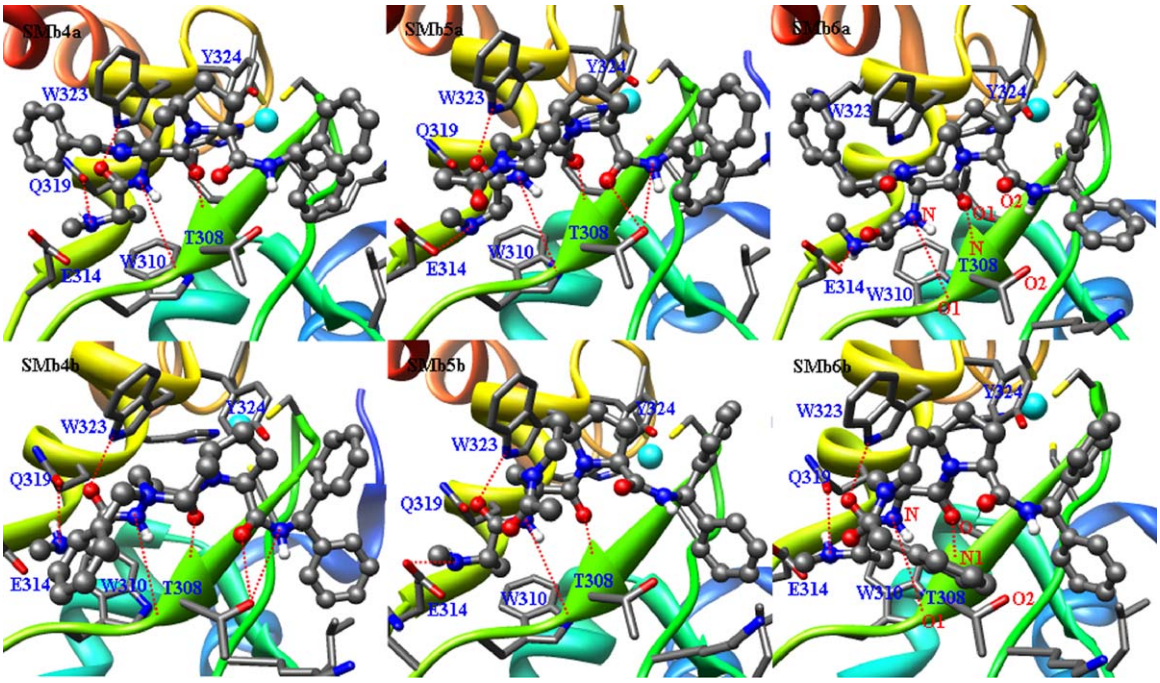

Fig. 4. Two docking conformations of each bicyclic core Smac mimetic with eight-membered ring SMb(4–6) bound to XIAP-BIR3. The red dashed lines represent hydrogen bonds. (For interpretation of the references to color in this figure legend, the reader is referred to the web version of the article.)

tetrahydroaphthyl is favorable to the binding, which is consistent with the result of SMa2.

However, when a benzyl is introduced into the five-membered ring, the binding energy of SMc3 is −11.66 kcal/mol. From the docking conformation in Fig. 5, one can see that the benzyl locates between the indole ring of Trp323 and the phenolic hydroxyl of Tyr324, which enhances the van der Waals contacts as well as hydrophobic interactions. The calculated energy including van der Waals, hydrogen bond and desolvation interaction changes from −9.20 to −11.96 kcal/mol. When the eight-membered ring bears a double bond (in SMc4), the benzyl ring is still in the original site and the binding affinity is almost unchanged.

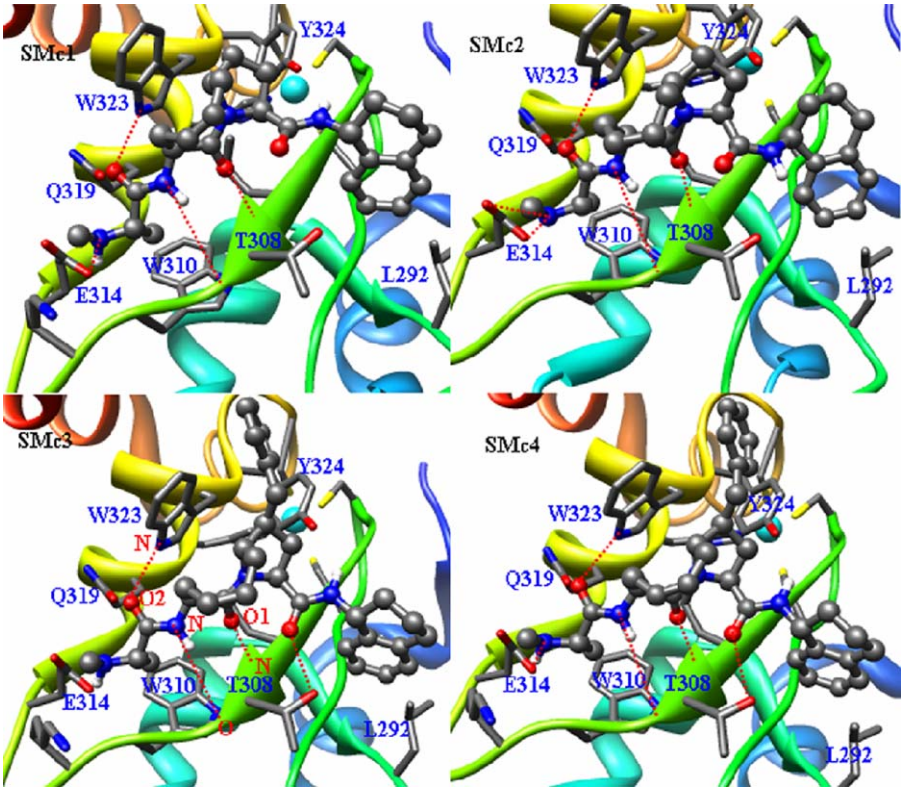

Fig. 5. The docking conformations of bicyclic core Smac mimetics SMc bound to XIAP-BIR3. The red dashed lines represent hydrogen bonds. (For interpretation of the references to color in this figure legend, the reader is referred to the web version of the article.)

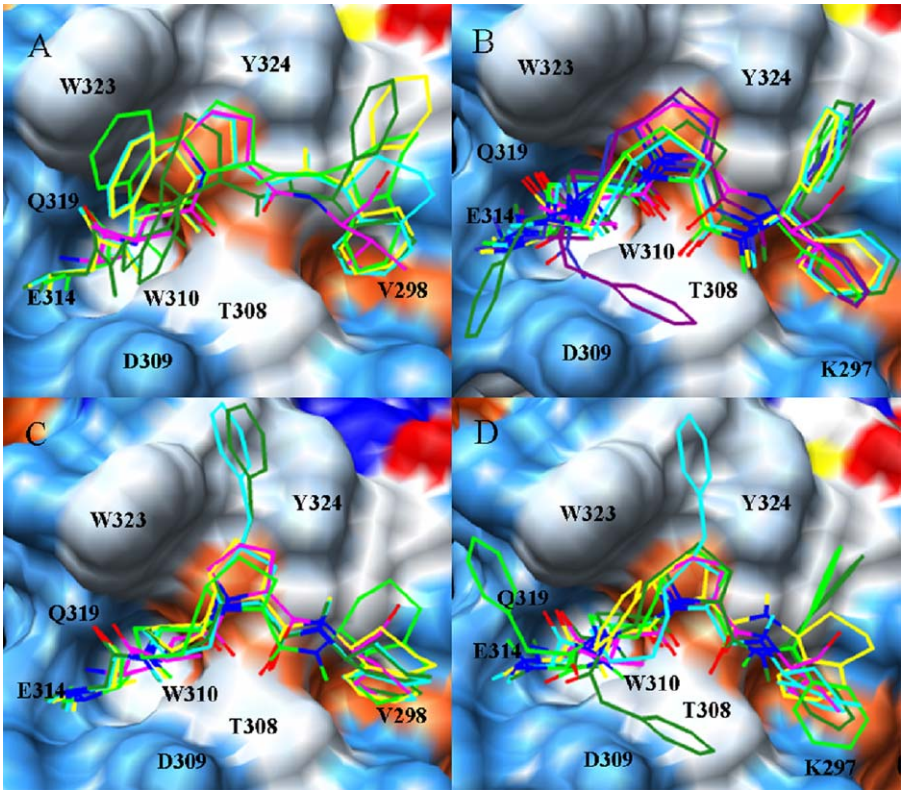

Fig. 6. Superpositions of docking conformations of Smac mimetics bound to the hydrophobic surface of XIAP-BIR3 domain. (A) SMa mimetics. Yellow for SMa1, cyan for SMa2, green for SMa3 and forest green for SMa4. (B) SMb mimetics. Yellow for SMb1, green for SMb2, cyan for SMb3, forest green for SMb4b, media blue for SMb5b and dark megmenta for SMb6b. (C) SMc mimetics. Yellow for SMc1, green for SMc2, cyan for SMc3 and forest green for SMc4. (D) Three typic Smac mimetics. Yellow for SMa2, green for SMb6a, forest green for SMb6b and cyan for SMc3. AVPI is shown in magenta. Oxygen atoms are colored in red and nitrogen atoms in blue. The hydrophobic surface shows amino acid hydrophobicity with colors ranging from dodger blue for the most hydrophilic to white at 0.0 to orange red for the most hydrophobic.

To better compare the positions and orientations of these mimetics on the surface groove, the docking conformations are superimposed on the hydrophobic surface of XIAP-BIR3, as shown in Fig. 6A–C. One can see that the backbones of these mimetics are superimposed together with that of AVPI. The most potent mimetics in each group, SMa2, SMb6 and SMc3, are also overlapped on the hydrophobic surface of XIAP-BIR3 (Fig. 6D). It indicates that the backbones are basically superimposed.

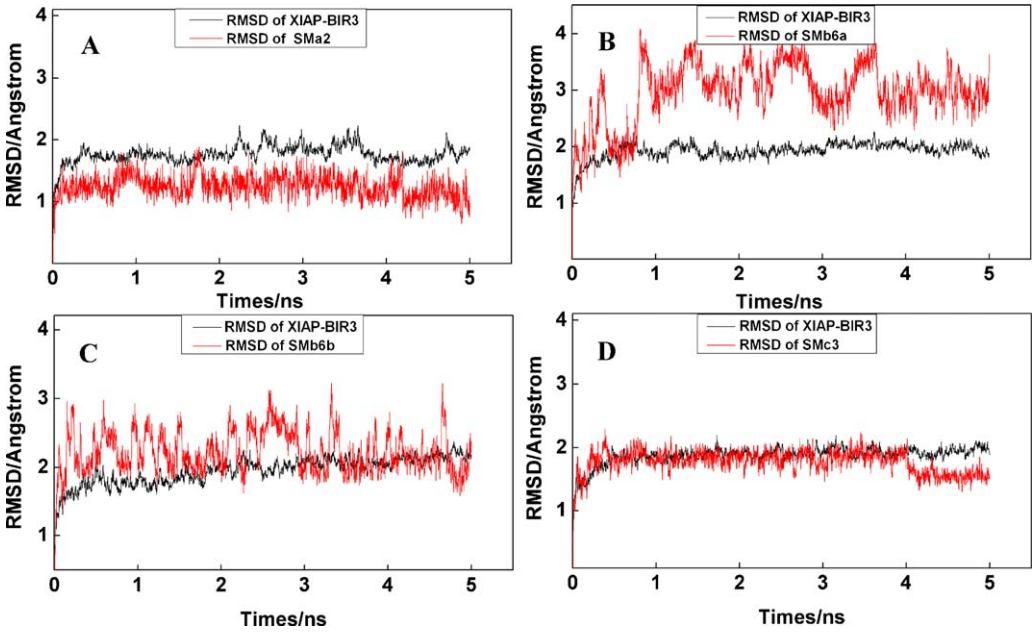

Fig. 7. Time dependences of RMSDs from XIAP-BIR3 domain and three typical Smac mimetics in 5 ns MD simulations.

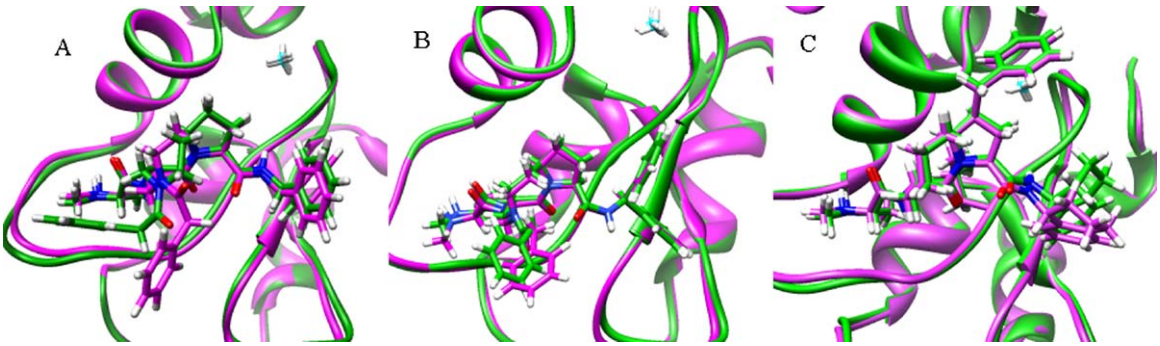

Fig. 8. The average structures of XIAP-BIR3 with SMb6a (A), SMb6b (B) and SMc3 (C) obtained from 5 ns MD simulations. (A) The structure from 0.5 to 1 ns is shown green, the one from 1 to 5 ns in magenta. (B) The structure from 0.5 to 3 nm is shown in green, the one from 3 to 5 nm in magenta. (C) The structure from 0.5 to 4 ns is shown in green, the one from 4 to 5 ns in magenta. Zinc ion in cyan. (For interpretation of the references to color in this figure legend, the reader is referred to the web version of the article.)

3.2. Molecular dynamics simulation

To study the stability and dynamics properties of mimetics interacting with XIAP-BIR3, based on the docking results, three mimetics with the best cell activity, SMa2, SMb6 and SMc3 bound to XIAP-BIR3, were selected to perform MD simulations, and MM_PBSA method was used to calculate the binding free energy.

The RMSDs of Smac mimetics and XIAP-BIR3 versus time are given in Fig. 7. It shows that the conformations of XIAP-BIR3 are stable in all simulations. The RMSD of SMa2 in Fig. 7A displays that it achieves equilibrium at 0.2 ns and afterwards stabilizes at 1.2 Å, indicating that the structure of SMa2 keeps stable during the simulations. In Fig. 7B, the RMSD of SMb6a is basically maintained at 3.0 Å but shows a great fluctuation. We examine the dynamics trajectory and find that the structure of SMb6a is changed during the simulations, which is given in Fig. 8A. We can see that the backbones of SMb6a are overlapped, but the positions of benzyl change a lot, which may be the main reason that the RMSD of SMb6a show large fluctuation. The starting conformation of SMb6a in Fig. 4 shows that the benzyl locates between the side chain of Gln319 and indole of Trp323, but it changes gradually during simulations and finally resides between Asp309 and Thr308. However, the RMSD of SMb6b in Fig. 7C is very smooth and keeps at 2.0 Å after 0.2 ns, and the average structures in Fig. 8B are overlapped well, indicating that SMb6b is more stable than SMb6a in dynamics simulations. From the RMSD of SMc3 in Fig. 7D, we find that SMc3 is stable in the binding pocket. The average structures of SMc3 in MD simulations are shown in Fig. 8C, which reveals that the position of R-tetrahydroaphthyl group changes during simulation.

In addition, we performed hydrogen bond analysis from the dynamics trajectories, which is listed in Table 3. The corresponding atomic labels are shown in Figs. 2, 4 and 5, respectively. It can be seen that the hydrogen bonds of these complexes mainly distributed between bicyclic core segment and Thr308 as well as carbonyl from amide and indole ring of Trp323. In particularly, the hydrogen bonds between Thr308 and bicyclic core segment are more stable with populations larger than 90% and 70%, respectively.

Energy terms contributing to the binding free energy by MM_PBSA method [39] are listed in Table 4. We can see that the major contributions to the binding free energy come from the van der Waals and electrostatic interactions for these four systems. However, the polar solvation free energies are unfavorable to the binding because of positive ΔG_{PBCAL} values (about ~50 kcal/mol), while the nonpolar solvation free energies (~−5 kcal/mol) provide similar favorable contribution to the binding. For two different conformations SMb6a and SMb6b, the major discrepancy comes from the electrostatic interaction energies (−36.40 *vs* −23.00 kcal/mol) and the polar solvation free energies (54.21 *vs* 41.25 kcal/mol), respectively. But their overall binding free energies are the same (−9.57 kcal/mol).

Fig. 9 gives the contribution of each residue of XIAP-BIR3 to the binding. It is noted that 10 residues are responsible for the binding, which are Lys297, Gly306, Leu307, Thr308, Asp309, Trp310, Lys311, Glu314, Gln319 and Trp323, respectively. In particular, three residues Thr308, Asp309 and Trp323 play important roles in interacting with the mimetics. This finding is well agreement with the previous result we drew [30].

Table 3
Intermolecular hydrogen bonds[a] between XIAP-BIR3 and mimetics in the MD simulations.

Mimetics	Donor	Acceptor H	Acceptor	Occupied (%)[b]	Average distance (Å)	Average angle (°)
SMa2	O(T308)	H(SMa2)	N(SMa2)	96.84	3.002	17.56
	O2(SMa2)	H(T308)	N(T308)	93.36	2.865	38.34
	O1(SMa2)	H(W323)	N(W323)	10.12	3.257	46.71
SMb6a	O1(SMb6)	H1(T308)	N(T308)	91.24	2.821	32.74
	O1(T308)	H(SMb6)	N(SMb6)	76.52	2.860	17.18
	O2(SMb6)	H2(T308)	O2(T308)	44.20	2.832	22.97
SMb6b	O(SMb6)	H1(T308)	N(T308)	88.28	2.755	18.76
	O(SMb6)	H2(T308)	O2(T308)	88.12	2.797	40.15
	O1(T308)	H(SMb6)	N(SMb6)	59.12	2.872	16.42
SMc3	O1(SMc3)	H(T308)	N(T308)	91.72	2.797	33.13
	O(T308)	H(SMc3)	N(SMc3)	71.68	2.866	15.59
	O2(SMc3)	H(W323)	N(W323)	38.44	2.859	31.82

[a] H-bond distance and angle cut-offs used in this study are 3.0 Å and 120°, respectively.
[b] The percentage of hydrogen bond population during the 5 ns MD simulations.

Table 4
Energy terms contributing to the binding free energy (kcal/mol) by the MM_PBSA.

Energy term	SMa2	SMb6a	SMb6b	SMc3
ΔE_{ELE}	−33.14	−36.40	−23.00	−30.47
ΔE_{VDW}	−42.70	−47.29	−44.31	−47.92
ΔE_{INT}	0.00	0.00	0.00	0.00
ΔE_{GAS}	−75.83	−83.68	−67.31	−78.39
ΔG_{PBSUR}	−5.48	−5.40	−5.24	−5.54
ΔG_{PBCAL}	48.94	54.21	41.25	47.09
ΔG_{PBSOL}	43.46	48.81	36.00	41.56
ΔG_{PBTOT}	−32.37	−34.88	−31.31	−36.83
$-T\Delta S_{TOT}$	25.16	25.31	21.74	22.59
$\Delta G_{PB,bind}$	−6.91	−9.57	−9.57	−14.24
$\Delta G_{exp,bind}$[a]	−10.55	−11.08	−11.08	−11.53

[a] The experimental data are calculated according to RT ln (K_i), T is 298 K in this study and K_i values are from Refs. [26–28]. ELE is the electrostatic energy, VDW is the van der Waals contribution, INT is the internal energy from bond, angle and dihedral terms in the MM force field. GAS = ELE + VDW + INT. PBSUR and PBCAL are nonpolar and polar contributions to the solvation free energy calculated by PB calculations, PBSOL = PBSUR + PBCAL, PBTOT = PBSOL + GAS. ΔS_{TOT} is the entropic contribution by nmode module.

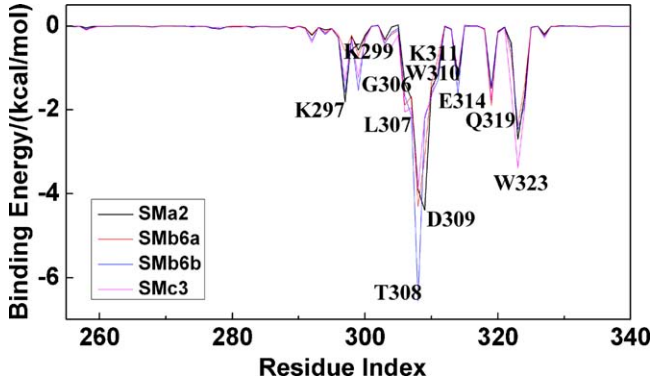

Fig. 9. Binding energy contribution of each residue of XIAP-BIR3 interacting with SMa2, SMb6a, SMb6b and SMc3, respectively. Only the key residues are given in the plot.

From the dynamics simulations we can see that the complex of SMc3 with XIAP-BIR3 is the most stable and the binding free energy is the lowest, therefore, introduction of a hydrophobic group into the five-membered ring is more favorable to the binding. The bicyclic core segment is very important for Smac mimetics interacting with XIAP-BIR3. On the one hand, it can make strong hydrogen bonds with Thr308 to maintain the stability of complex; on the other hand, it can contact with the hydrophobic surface between Trp323 and Tyr324, simultaneously it forms van der Waals interactions with the indole ring of Trp323. These interactions enhance the binding between mimetics and XIAP-BIR3.

4. Conclusions

Molecular docking and dynamics simulations were performed to investigate the binding of three groups of Smac mimetics to XIAP-BIR3. The docking results show that all these Smac mimetics can be docked into the surface groove. A phenyl fused to the seven-membered ring of bicyclic core contributes a little to the binding because of steric hindrance; the steric exclusion of the eight-membered ring in SMb decreases the binding affinity. The terminal R-tetrahydronaphtyl group increases the hydrophobic interactions and benefits the ligand binding; especially a benzyl on five-membered ring of SMc3 provides remarkable contribution to the binding for its van der Waals and hydrophobic interactions.

Molecular dynamics simulations on three typical complexes show that the backbones of SMb6 and SMc3 are essentially stable, but the phenyl of SMb6a keeps away from the indole ring of Trp323 and closes to the side chain of Asp309 gradually, indicating that SMb6a would convert its conformation to SMb6b, while the benzyl of SMc3 changes slightly. Hydrogen bond analysis further reveals that the hydrogen bonds between bicyclic core segment and Thr308 play a critical role in maintaining the stability of complex. The binding free energies calculated by MM_PBSA method are in agreement with the experimental results.

Acknowledgements

This work was supported by the National Natural Science Foundation of China (20873075, 20633060) and Independent Innovation Foundation of Shandong University (2009JC018).

References

[1] M.O. Hengartner, Programmed cell death in invertebrates, Curr. Opin. Genet. Dev. (1996) 634–638.
[2] M.D. Jacobson, M. Weil, M.C. Raff, Programmed cell death in animal development, Cell 88 (1997) 347–354.
[3] Y. Shi, Mechanisms of caspase activation and inhibition during apoptosis, Mol. Cell 9 (2002) 459–470.
[4] D.W. Nicholson, Caspases structure, proteolytic substrates and function during apoptotic cell death, Cell Death Differ. 6 (1999) 1028–1042.
[5] Y. Shi, A structural view of mitochondria-mediated apoptosis, Nat. Struct. Biol. 8 (2001) 394–401.
[6] Y. Huang, R.L. Rich, D.G. Myszka, H. Wu, Requirement of both the second and third BIR domains for the relief of X-linked inhibitor of apoptosis protein (XIAP)-mediated caspase inhibition by Smac, J. Biol. Chem. 278 (2003) 49517–49522.
[7] E.N. Shiozaki, J. Chai, D.J. Rigotti, S.J. Riedl, P. Li, S.M. Srinivasula, E.S. Alnemri, R. Fairman, Y. Shi, Mechanism of XIAP-mediated inhibition of caspase-9, Mol. Cell 11 (2003) 519–527.
[8] C. Du, M. Fang, Y. Li, L. Li, X. Wang, Smac, a mitochondrial protein that promotes cytochrome c-dependent caspase activation by eliminating IAP inhibition, Cell 102 (2000) 33–42.
[9] A.M. Verhagen, P.G. Ekert, M. Pakusch, J. Silke, L.M. Connolly, G.E. Reid, R.L. Moritz, R.J. Simpson, D.L. Vaux, Identification of DIABLO, a mammalian protein that promotes apoptosis by binding to and antagonizing IAP proteins, Cell 102 (2000) 43–53.
[10] Z. Liu, C. Sun, E.T. Olejniczak, R.P. Meadows, S.F. Betz, T. Oost, J. Herrmann, J.C. Wu, S.W. Fesik, Structural basis for binding of Smac/DIABLO to the XIAP BIR3 domain, Nature 408 (2000) 1004–1008.
[11] G. Wu, J. Chai, T.L. Suber, J. Wu, C. Du, X. Wang, Y. Shi, Structural basis of IAP recognition by Smac/DIABLO, Nature 408 (2000) 1008–1012.
[12] S.M. Srinivasula, R. Hegde, A. Saleh, P. Datta, E. Shiozaki, J. Chai, R. Lee, P.D. Robbins, T. Fernandes-Alnemri, Y. Shi, E.S. Alnemri, A conserved XIAP-interaction motif in caspase-9 and Smac/DIABLO regulates caspase activity and apoptosis, Nature 410 (2001) 112–116.
[13] R.A. Kipp, M.A. Case, A.D. Wist, C.M. Cresson, E. Griner, A. Wiita, P.A. Albiniak, J. Chai, Y. Shi, M.F. Semmelhack, G.L. McLendon, Molecular targeting of inhibitor of apoptosis proteins based on small molecule mimics of natural binding partners, Biochemistry 41 (2002) 7344–7349.
[14] H. Sun, Z. Nikolovska-Coleska, C. Yang, D. Qian, J. Lu, S. Qiu, L. Bai, Y. Peng, Q. Cai, S. Wang, Design of small-molecule peptidic and nonpeptidic Smac mimetics, Acc. Chem. Res. 41 (2008) 1264–1277.
[15] C. Park, C. Sun, E.T. Olejniczak, A.E. Wilson, R.P. Meadows, S.F. Betz, S.W. Elmore, S.W. Fisk, Non-peptidic small molecule inhibitors of XIAP, Bioorg. Med. Chem. Lett. 15 (2005) 771–775.
[16] P. Seneci, A. Bianchi, C. Battaglia, L. Belvisi, M. Bolognesi, A. Caprini, F. Cossu, E. de Franco, M. de Matteo, D. Delia, C. Drago, A. Khaled, D. Lecis, L. Manzoni, M. Matizzoni, E. Mastrangelo, M. Milani, I. Motto, E. Moroni, D. Potenza, V. Rizzo, F. Servida, E. Turlizzi, M. Varrone, F. Vasile, C. Scolastico, Rational design, synthesis and characterization of potent, non-peptidic Smac mimics/XIAP inhibitors as proapoptotic agents for cancer therapy, Bioorg. Med. Chem. 17 (2009) 5834–5856.
[17] J. Huang, Z. Zhang, B. Wu, J.F. Cellitti, X. Zhang, R. Dahl, C. Shiau, K. Welsh, A. Emdadi, J.L. Stebbins, J.C. Reed, M. Pellecchia, Fragment-based design of small molecule X-linked inhibitor of apoptosis protein inhibitors, J. Med. Chem. 51 (2008) 7111–7118.
[18] F. Cossu, E. Mastrangelo, M. Milani, G. Sorrentino, D. Lecis, D. Delia, L. Manzoni, P. Seneci, C. Scolastico, M. Bolognesi, Designing Smac-mimetics as antagonists of XIAP, cIAP1 and cIAP2, Biochem. Biophys. Res. Commun. 378 (2009) 162–167.
[19] H. Sun, Z. Nikolovska-Coleska, J. Lu, J.L. Meagher, C. Yang, S. Qiu, Y. Tomita, Y. Ueda, S. Jiang, K. Krajewski, P.P. Roller, J.A. Stuchey, S. Wang, Design, synthesis, and characterization of a potent, nonpeptide, cell-permeable, bivalent Smac mimetics that concurrently targets both the BIR2 and BIR3 domains in XIAP, J. Am. Chem. Soc. 129 (2007) 15279–15294.
[20] Z. Nikolovska-Coleska, J.L. Meagher, S. Jiang, C. Yang, S. Qiu, P.P. Roller, J.A. Stuckey, S. Wang, Interaction of a cyclic, bivalent Smac mimetic with the X-linked inhibitor of apoptosis protein, Biochemistry 47 (2008) 9811–9824.

[21] F. Cossu, M. Milani, E. Mastrangelo, P. Vachette, F. Servida, D. Lecis, G. Canevari, D. Delia, C. Drago, V. Rizzo, L. Manzoni, P. Sceneci, C. Scolastico, M. Bolognesi, Structural basis for bivalent Smac-mimetics recognition in the IAP protein family, J. Mol. Biol. 392 (2009) 630–644.
[22] H. Sun, J.A. Stuckey, Z. Nikolovska-Coleska, D. Qin, J.L. Meagher, S. Qiu, J. Lu, C. Yang, N. Saito, S. Wang, Structure-based design, synthesis, evaluation, and crystallographic studies of conformationally constrained Smac mimetics as inhibitors of the X-linked inhibitor of apoptosis protein (XIAP), J. Med. Chem. 51 (2008) 7169–7180.
[23] H. Sun, Z. Nikolovska-Coleska, C. Yang, L. Xu, M. Liu, Y. Tomita, H. Pan, Y. Yoshioka, K. Krajewski, P.P. Roller, S. Wang, Structure-based design of potent, conformationally constrained Smac mimetics, J. Am. Chem. Soc. 126 (2004) 13386–16687.
[24] H. Sun, Z. Nikolovska-Coleska, C. Yang, L. Xu, Y. Tomita, K. Krajewski, P.P. Roller, S. Wang, Structure-based design, synthesis, and evaluation of conformationally constrained mimetics of the second mitochondria-derived activator of caspase that target the X-linked inhibitor of apoptosis protein/caspase-9 interaction site, J. Med. Chem. 47 (2004) 4147–4150.
[25] H. Sun, Z. Nikolovska-Coleska, J. Lu, S. Qiu, C. Yang, J. Meagher, J. Stuckey, S. Wang, Cell-permeable, conformationally constrained second mitochondria derived activator of caspase (Smac) mimetic, J. Med. Chem. 49 (2006) 7916–7920.
[26] B. Zhang, Z. Nikolovska-Coleska, Y. Zhang, L. Bai, S. Qiu, C. Yang, H. Sun, S. Wang, Y. Wu, Design, synthesis, and evaluation of tricyclic, conformationally constrained small-molecule minetics of second mitochondria-derived activator of caspases, J. Med. Chem. 51 (2008) 7352–7355.
[27] Y. Peng, H. Sun, Z. Nikolovska-Coleska, S. Qiu, C. Yang, J. Lu, Q. Cai, H. Yi, S. Kang, D. Yang, S. Wang, Potent, orally bioavailable diazabicyclic small-molecule mimetics of second mitochondria-derived activator of caspases, J. Med. Chem. 51 (2008) 8158–8162.
[28] W. Sun, Z. Nikolovska-Coleska, D. Qin, H. Sun, C. Yang, L. Bai, S. Qiu, Y. Wang, D. Ma, S. Wang, Design, synthesis, and evaluation of potent, nonpeptidic mimetics of second mitochondria-derived activator of caspases, J. Med. Chem. 52 (2009) 593–596.
[29] C. Yang, H. Sun, J. Chen, Z. Nikolovska-Coleska, S. Wang, Importance of ligand reorganization free energy in protein-ligand binding-affinity prediction, J. Am. Chem. Soc. 131 (2009) 13709–13721.
[30] B. Ling, R. Zhang, Z. Wang, Y. Liu, C. Liu, Study on the interactions of Smac mimetics with XIAP-BIR3 by docking and molecular dynamics simulations. J. Theor. Comput. Chem., in press.
[31] M.J. Frisch, G.W. Trucks, H.B. Schlegel, G.E. Scuseria, M.A. Robb, J.R. Cheeseman, J.A. Montgomery, T. Vreven Jr., K.N. Kudin, J.C. Burant, J.M. Millam, S.S. Iyengar, J. Tomasi, V. Barone, B. Mennucci, M. Cossi, G. Scalmani, N. Rega, G.A. Petersson, H. Nakatsuji, M. Hada, M. Ehara, K. Toyota, R. Fukuda, J. Hasegawa, M. Ishida, T. Nakajima, Y. Honda, O. Kitao, H. Nakai, M. Klene, X. Li, J.E. Knox, H.P. Hratchian, J.B. Cross, V. Bakken, C. Adamo, J. Jaramillo, R. Gomperts, R.E. Stratmann, O. Yazyev, A.J. Austin, R. Cammi, C. Pomelli, J.W. Ochterski, P.Y. Ayala, K. Morokuma, G.A. Voth, P. Salvador, J.J. Dannenberg, V.G. Zakrzewski, S. Dapprich, A.D. Daniels, M.C. Strain, O. Farkas, D.K. Malick, A.D. Rabuck, K. Raghavachari, J.B. Foresman, J.V. Ortiz, Q. Cui, A.G. Baboul, S. Clifford, J. Cioslowski, B.B. Stefanov, G. Liu, A. Liashenko, P. Piskorz, I. Komaromi, R.L. Martin, D.J. Fox, T. Keith, M.A. Al-Laham, C.Y. Peng, A. Nanayakkara, M. Challacombe, P.M.W. Gill, B. Johnson, W. Chen, M.W. Wong, C. Gonzalez, J.A. Pople, Gaussian 03, Revision C. 02, Gaussian, Inc., Wallingford CT, 2004.
[32] G.M. Morris, D.S. Goodsell, R.S. Halliday, R. Huey, W.E. Hart, R.K. Belew, A.J. Olson, Automated docking using a Lamarckian genetic algorithm and an empirical binding free energy function, J. Comput. Chem. 19 (1998) 1639–1662.
[33] S.Y. Lu, Y.J. Jiang, J. Lv, T.X. Wu, Q.S. Yu, W.L. Zhu, Molecular docking and molecular dynamics simulation studies of GPR40 receptor-agonist interactions, J. Mol. Graph. Model. 28 (2010) 766–774.
[34] D.A. Case, T.A. Darden, T.E. Cheatham, C.L. Simmerling III, J. Wang, R.E. Duke, R. Luo, K.M. Merz, D.A. Pearlman, M. Crowley, R.C. Walker, W. Zhang, B. Wang, S. Hayik, A. Roitberg, G. Seabra, K.F. Wong, F. Paesani, X. Wu, S. Brozell, V. Tsui, H. Gohlke, L. Yang, C. Tan, J. Mongan, V. Hornak, G. Cui, P. Beroza, D.H. Mathews, C. Schafmeister, W.S. Ross, P.A. Kollman, AMBER 9, University of California, San Francisco, 2006.
[35] E. Papaleo, L. Russo, N. Shaikh, L. Cipolla, P. Fantucci, L. De Gioia, Molecular dynamics investigation of cyclic natriuretic peptides: dynamics properties reflect peptide activity, J. Mol. Graph. Model. 28 (2010) 834–841.
[36] J.L. Klepeis, Lindorff-Larsen, R.O. Dror, D.E. Shaw, Long-timescale molecular dynamics simulations of protein structure and function, Curr. Opin. Struct. Biol. 19 (2009) 120–127.
[37] Y. Pang, Novel Zinc protein molecular dynamics simulations: steps toward antiangiogenesis for cancer treatment, J. Mol. Model. 5 (1999) 196–202.
[38] Y. Pang, Successful molecular dynamics simulation of two zinc complexes bridged by a hydroxide in phosphotriesterase using the cationic dummy atom method, Proteins 45 (2001) 183–189.
[39] P.A. Kollman, I. Massova, C. Reyes, B. Kuhn, S. Huo, L. Chong, M. Lee, T. Lee, Y. Duan, W. Wang, O. Donini, P. Cieplak, J. Srinivasan, D.A. Case, T.E. Cheatham III, Acc. Chem. Res. 33 (2000) 889–897.
[40] C. Obiol-Pardo, J. Rubio-Martinez, Comparative evaluation of MMPBSA and XSCORE to compute binding free energy in XIAP-peptide complex, J. Chem. Inf. Model. 47 (2007) 134–142.
[41] T. Li, M. Froeyen, P. Herdewijn, Computational alanine scanning and free energy decomposition for *E.* Coli type I signal peptidase with lipopeptide inhibitor complex, J. Mol. Graph. Model. 26 (2008) 813–823.
[42] E. Mastrangelo, F. Cossu, M. Milani, G. Sorrentino, D. Lecis, D. Dellia, L. Manzoni, P. Seneci, C. Scolastico, V. Rizzo, M. Bolognesi, Targeting the X-linked inhibitor of apoptosis protein through 4-substituted azabicylo[5.3.0]alkane Smac mimetics. Structure, activity and recognition principles, J. Mol. Biol. 384 (2008) 673–689.
[43] E.F. Pettersen, T.D. Goddard, C.C. Huang, G.S. Couch, D.M. Greenblatt, E.C. Meng, T.E. Ferrin, UCSF chimera – a visualization system for exploratory research and analysis, J. Comput. Chem. 25 (2004) 1605–1612.